Outline Version — 2017 April 23
Preprint typeset using LaTeX style emulateapj v. 12/16/11

A MID-IR SELECTED CHANGING-LOOK QUASAR

DANIEL STERN[1] ET AL.

Outline Version — 2017 April 23

ABSTRACT

We report a new changing-look quasar, WISE J105203.55+151929.4 at $z = 0.303$, found by identifying highly mid-IR variable quasars in the the *WISE/NEOWISE(R)* data stream. Compared to multi-epoch mid-IR photometry of a large sample of SDSS-confirmed quasars, WISE J1052+1519 is an extreme outlier, fading by more than a factor of two at 3.4 and 4.6μm since 2009. Our recent *Swift* target-of-opportunity observations show comparable fading in the soft X-rays compared to the *ROSAT* detection of this source in 199X. We obtained second-epoch spectroscopy with the Palomar telescope in January 2017, which, when compared with the 2006 archival SDSS spectrum, reveals that the broad Hβ emission has vanished and that the quasar has become significantly redder. The two most likely interpretations for this dramatic change are source fading or obscuration, where the former is strongly favored by the mid-IR data. We discuss various physical scenarios that could cause such dramatic changes in the quasar fueling over a short time-scale, and predict the multiwavelength signatures that could distinguish these phenomena.

Keywords: galaxies: active — quasars: individual (WISE J105203.55+151929.4)

1. INTRODUCTION

[*Daniel: Summarize recent literature on changing-look quasars (e.g. LaMassa et al. 2015; Macleod et al. 2016; Gezari et al. 2017; Stern et al. 2017) — and mention NuSTAR-identified changing-look quasar buried in Alexander et al. (2013), as well as curmudgeonly discussion of decades-long knowledge of such events, from X-rays (e.g. Risaliti et al. 2002), in Seyferts (REF), and 3C303 (Arjun - REF?). Briefly describe WISE/NEOWISE, and emphasize that this is the first changing-look quasar selected from mid-IR data, which provides an additional, powerful tool for distinguishing between a fading AGN and increased obscuration of the central engine.*]

2. OBSERVATIONS

2.1. *Selection of WISE J1052+1519*

Mid-infrared $W1$ (3.4 μm) and $W2$ (4.6 μm) lightcurves for $\sim$200,000 SDSS spectroscopic quasars were extracted from Data Release 3 (DR3) of the Dark Energy Camera (DECam; REF?) Legacy Survey (DECaLS; REF?). These light curves span the period from the beginning of the *WISE* mission (Wright et al. 2010) in 2010 January through 2014 December, corresponding to the first-year of *NEOWISER* operations (Mainzer et al. 2014). Note that no data is available between 2011 February and 2013 September, when the *WISE* satellite was in hibernation. A given sky location is observed by *WISE* for $\sim$1 day once every six months, which means that we typically have four epochs of photometry available, separated by a minimum of six months and a maximum of four years. The $W1/W2$ light curves were obtained by performing forced photometry at the locations of DECam-detected optical sources on time-resolved un*WISE* co-adds (Lang 2014; Lang et al. 2016), each of which represents a stack with depth of coverage $\sim$12 exposures. While this approach means that we cannot probe variability on timescales less than 1 day, the co-adds allow photometry 1.4 mag deeper than the individual exposures and removes virtually all single-exposure artifacts (e.g., cosmic rays and satellites).

Approximately 30,000 of the SDSS quasars with such $W1/W2$ lightcurves available are "IR-bright", in the sense that they are above both the $W1$ and $W2$ single exposure thresholds and therefore detected at very high significance in our co-adds. For this ensemble of objects, the typical variation in each quasar's measured $(W1-W2)$ color is 0.06 magnitudes, which includes statistical and systematic errors expected to contribute variations at the few hundredths of a magnitude level. The typical measured single-band scatter is 0.07 magnitudes in each of $W1$ and $W2$. A full characterization of the typical mid-IR quasar variability will be presented separately (Ross et al., in preparation).

[*Note from Arjun: Can we be more quantitative, since much depends on the luminosity and color and redshift of the QSOs in the SDSS sample. Perhaps this is for Aaron's sample description paper (which we should reference here), but we could at least mention the range of W1-W2 and perhaps r-W1 of the detected sample.*]

We undertook a search for extreme outliers relative to these trends. Specifically, we selected objects with the following characterisitcs.

- Monotonic variation in both $W1$ and $W2$.
- $W1$ versus $W2$ flux correlation coefficient $>$0.9.
- $>$ 0.5 mag peak-to-peak variation in either $W1$ or $W2$.

This yielded a sample of 248 sources, of which 31 are assumed to be blazars due to the presence of radio counterparts from the Faint Images of the Radio Sky at Twenty cm survey (FIRST; Becker et al. 1995). Another 22 are outside the FIRST footprint, leaving 195 radio-undetetected ($S_{1.4\ \mathrm{GHz}} \lesssim 1$ mJy; 5σ) quasars in our IR-variable sample. We randomly selected five of these objects for follow-up spectroscopy with Palomar on the night of UT 2017 January 30. WISE J1052+1519, one of these five, faded by 0.75 (0.9)

[1] Jet Propulsion Laboratory, California Institute of Technology, 4800 Oak Grove Drive, Mail Stop 169-221, Pasadena, CA 91109, USA [e-mail: daniel.k.stern@jpl.nasa.gov]

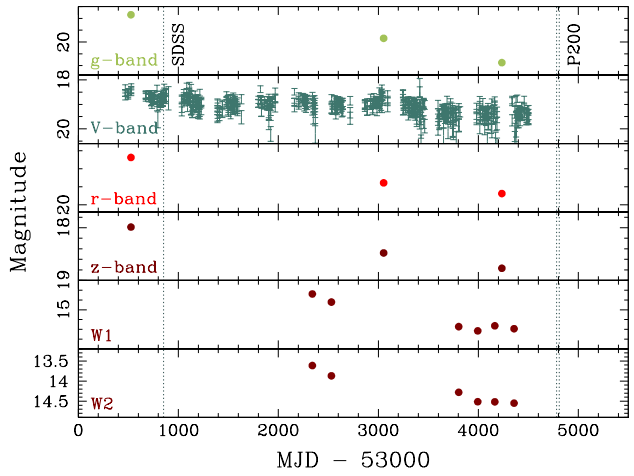

Figure 1. Multi-wavelength lightcurves, with vertical dotted lines showing the epochs of the spectroscopy. See text and Table table:photometry for details. *V*-band photometry is from the unfiltered CCD observations by CRTS (for details, see Drake et al. 2009).

mags in $W1$ ($W2$) between 2010 May and 2014 December, and thus became 0.15 mags bluer in $(W1-W2)$, making it a significant outlier in both single-band and IR color variability.

2.2. *UV to Mid-IR Photometry and Lightcurve*

Figure 1 presents a multi-wavelength lightcurve of this source, including optical data from SDSS, Pan-STARRS, DECaLS, and the Catalina Real-time Transient Survey (CRTS; Drake et al. 2009), as well as the mid-infrared photometry discussed above. We have also supplemented the DECaLS DR3 $W1/W2$ light curves with *NEOWISER* epochal co-adds between 2015 May and 2015 December, providing two additional mid-infrared photometric epochs to the light curve in Figure 1. Much of this data is presented in Table 1, which also includes the single-epoch UV photometry from the *Galaxy Evolution Explorer* (*GALEX*; Martin et al. 2005), and near-IR photometry from the Two Micron All Sky Survey (Skrutskie et al. 2006).

Overall, the WISE J1052+1519 has shown significant fading in the past decade, at both optical and mid-infrared wavelengths. Optically, the sources has changed most at the bluest wavelengths, fading by 1.8 mag at *g*-band between SDSS and DeCaLS, though only by 1.0 mag at *r*-band and 0.8 mag at *z*-band. In the infrared, the situation is reversed, with the more significant fading occuring in the redder $W2$ band, by 0.9 mag, while the bluer $W1$ band faded by only 0.7 mag. Since galaxy spectra peak in the near-infrared, while AGN spectra are, to first order, power-laws in this wavelength and thus become most evident in the rest-frame UV and longwards of a few microns, the observed temporal evolution of WISE J1052+1519 is consistent with a dramatic decrease in its AGN emission.

2.3. *Spectroscopy*

WISE J1052+1519 was first observed spectroscopically by SDSS on UT 2006 April 27 (MJD = 53852; Blanton et al. 2003). The spectrum, shown in Figure 2, reveals a typical quasar with broadened emission lines from multiple hydrogen Balmer transitions (i.e., Hα through Hδ), strong, narrow emisison from the [O II] and [O III] doublets, and strong blue

Table 1

Band	MJD	Magnitude	Survey
FUV	53798	20.24 ± 0.23	*GALEX*
NUV	53798	19.78 ± 0.07	*GALEX*
u	53526	19.048 ± 0.024	SDSS
g	53526	18.848 ± 0.010	SDSS
r	53526	18.688 ± 0.010	SDSS
i	53526	18.619 ± 0.012	SDSS
z	53526	17.987 ± 0.022	SDSS
g	56053	19.846 ± 0.092	Pan-STARRS
r	56053	19.392 ± 0.029	Pan-STARRS
i	56053	19.084 ± 0.047	Pan-STARRS
z	56053	18.479 ± 0.033	Pan-STARRS
y	56053	18.597 ± 0.101	Pan-STARRS
g	57401	20.876 ± 0.021	DECaLS DR3
r	57401	19.690 ± 0.012	DECaLS DR3
z	57447	18.769 ± 0.007	DECaLS DR3
J	50798	16.823 ± 0.116	2MASS
H	50798	16.081 ± 0.151	2MASS
K_s	50798	15.529 ± 0.166	2MASS
$W1$	⟨55435⟩	14.752 ± 0.033	AllWISE
$W2$	⟨55435⟩	13.760 ± 0.038	AllWISE
$W3$	⟨55435⟩	11.340 ± 0.172	AllWISE
$W4$	⟨55435⟩	8.229 ± 0.267	AllWISE
$W1$	55340	14.677 ± 0.018	un*WISE*
$W2$	55340	13.614 ± 0.026	un*WISE*
$W1$	55531	14.843 ± 0.021	un*WISE*
$W2$	55531	13.870 ± 0.031	un*WISE*
$W1$	56804	15.346 ± 0.034	un*WISE*
$W2$	56804	14.279 ± 0.053	un*WISE*
$W1$	56994	15.432 ± 0.038	un*WISE*
$W2$	56994	14.513 ± 0.072	un*WISE*
$W1$	57165	15.328 ± 0.077	un*WISE*
$W2$	57165	14.516 ± 0.141	un*WISE*
$W1$	57357	15.388 ± 0.096	un*WISE*
$W2$	57357	14.548 ± 0.180	un*WISE*

Note. — Photomtry is in its native system; i.e., optical photometry is in the AB system, while near-/mid-IR photometry is in the Vega system. *GALEX* MJD date is `meanObsMJD` and Pan-STARRS MJD date is `epochMean` from their data releases, respectively, while the AllWISE MJD date is the average of the first two *WISE* passes. [*Perhaps don't include table in paper, but this is useful for SED modeling (§3.1).*]

continuum rising below ~ 5500 Å. SDSS reports a redshift of $z = 0.303$ for the source, and classifies it as a quasar.

Because of its unusual lightcurve, we obtained additional optical spectroscopy of WISE J1052+1519 using the Double Spectrograph (DBSP) on the Hale 200" Telescope at Palomar Observatory on UT 2017 January 30 (MJD = 57783). We obtained a single 900 s observation of the target using the $1\farcs5$ slit. The night was photometric, though extremely windy leading to highly variable seeing that exceeded $3''$ at times. This effectively made the night non-photometric, as well as significantly impacted the quality of the data from that night. We processed the data using standard procedures and flux calibrated the spectrum with observations of the white dwarf spectrophotometric standard stars G191-B2B and HZ44 from Massey & Gronwall (1990) obtained on the same night. Though with limited signal-to-noise ratio, the January spectrum showed a spectrum with significantly less rest-frame UV/blue emission, and much weak Balmer emission, suggesting a highly dramatic spectral change since the SDSS data from a decade earlier.

In order to improve the signal-to-noise ratio, we re-observed WISE J1052+1519 with DBSP on the Palomar 200" on UT 2017 February 25 (MJD = 57809). We obtained two 600 s observations through the $1\farcs5$ slit in photometric, good-seeing conditions. The February data were flux calibrated

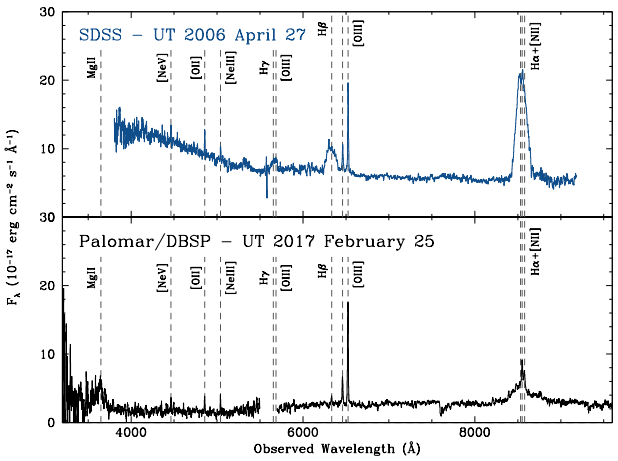

Figure 2. Multi-epoch optical spectra of WISE J1052+1519. Top panel shows the SDSS spectrum from Spring 2006, while lower panel shows the Palomar spectrum from Winter 2017. Key emission lines are labelled. In the past decade, the continuum has become significantly less blue, and higher order Balmer lines are no longer visible.

with observations of the spectrophotometric standards HZ14 and Feige 56 observed on that same night. Figure 2 presents the February Palomar data, which is of significantly better quality than the January Palomar spectrum.

Comparing the SDSS and Palomar spectra, we see that the source has faded significantly over the past decade. The rising blue continuum is no longer evident, nor are any of the broad Balmer emission lines other than Hα. Broad Mg II is visible in the Palomar, blue-ward of the spectral range of the SDSS data so not available for direct investigation of temporal evolution. The narrow [O III] lines are slightly weaker in the Palomar data at the few tens of percent level. Since the narrow-line region of quasars are typically spatially extended on scales of tens to thousands of parsecs, this difference is likely due to larger, 3″ diameter fiber used by SDSS compared to the 1.″5 wide slit used at Palomar.

2.4. *X-Ray Observations*

Fortuitously, WISE J1052+1519 resides 40.6′ from the spiral galaxy MCG+03-28-022 ($z = 0.022$), which hosted the exceptionally luminous type II supernova SN 1998Z. This supernova is believed to have exploded in a high-density environment, perhaps associated with mass loss from its high-mass progenitor (Stathakis & Sadler 1991). At the time, it was the most distant and most luminous supernova detected at both radio (Van Dyk et al. 1993) and X-ray energies, where the latter came from targeted 12.3 ks observation with *ROSAT* in 1995 May (Fabian & Terlevich 1996). WISE J1052+1519 was serendipitously detected in those X-ray data, and is listed in the Second *ROSAT* All-Sky Survey (Boller et al. 2016) as 2RXS J105203.9+151930, with a 0.1–2.4 keV flux of 1.3×10^{-12} erg cm^{-2} s^{-1} (assuming a power-law fit to the X-ray spectrum).

This relatively bright archival detection of our quasar prior to its optical fading inspired a successful *Swift* Target of Opporunity proposal to study how it has evolved at higher energies. *Swift* observed WISE J1052+1519 with the X-Ray Telescope (XRT; Burrows et al. 2005) and Ultraviolet/Optical Telescope (UVOT; Roming et al. 2005) instruments starting on UT 2017 February 17 (obsID 00034933001). We processed the raw data using the online analysis tools provided by the ASI Science Data Center[2]. HEAsoft version 6.20 and CALDB version 20111031 were used for data reduction and calibration. The total exposure was 4.3 ks with *Swift*/XRT, and 3.3 ks with *Swift*/UVOT (after coadding five separate frames taken with the UVM2 filter).

No X-ray source was detected at the coordinates of the *ROSAT* counterpart of WISE J1052+1519. The nearest detected source (SNR=4.4) is at 10:51:50.46, +15:17:53.26, with a 0.3–10 keV count rate of $(6.0 \pm 1.4) \times 10^{-3}$ s^{-1}. Nearby 2-sigma detected sources have count rates $(1.3 \pm 0.7) \times 10^{-3}$ s^{-1} and $(1.6 \pm 0.8) \times 10^{-3}$ s^{-1}. We therefore estimate a 3-sigma upper limit on the count rate of W1052+1519 to be 3×10^{-3} s^{-1} in the 0.3–10 keV band. Assuming a simple unabsorbed power-law spectrum with a photon index $\Gamma = 2$, this corresponds to a flux limit of 1.07×10^{-13} erg cm^{-2} s^{-1} in the 0.3–10 keV band, and 4.90×10^{-14} erg cm^{-2} s^{-1} in the 2–10 keV band. Alternatively, for a softer $\Gamma = 2.5$ spectrum, the corresponding limits are 8.89×10^{-14} erg cm^{-2} s^{-1} and 2.30×10^{-14} erg cm^{-2} s^{-1}, respectively. This conversion to flux includes the Galactic column density, $N_{\rm H} = 2.3 \times 10^{20}$ cm^{-2} (Kalberla et al. 2005). The X-ray non-detection implies that WISE J1052+1519 has faded by at least an order of magnitude in the past two decades.

The target is detected at low significance ($\lesssim 5$ sigma) in the *Swift*/UVOT UVM2 image at coordinates 10:52:03.5, +15:19:28.9. From aperture photometry, using a 5-pixel (1.8-arcsec) radius, we estimate the source magnitude to be 21.2 ± 0.3 in the UVM2 filter ($\lambda_{\rm eff} = 2231$ Å). The background was determined from an annulus with an inner radius of 15 and outer radius of 30 pixels, including no other sources. Correcting for the reddening along the line of sight (E(B−V)=0.026; Schlafly & Finkbeiner 2011), we find a flux density of $(3.12 \pm 0.81) \times 10^{-6}$ Jy.

3. DISCUSSION

3.1. *Black Hole Mass and Eddington Ratio*

From the SDSS spectrum, Shen et al. (2011) measure the Hα emission line has a full-width at half-maximum FWHM(Hα) = 5113 ± 129 km s^{-1}, FWHM(Hβ) = 5622 ± 145 km s^{-1}, a 5100 Å continuum luminosity of $\log L(5100)/({\rm erg\,s^{-1}}) = 44.107 \pm 0.004$, and an H$\alpha$ luminosity of $\log L({\rm H}\alpha)/({\rm erg\,s^{-1}}) = 42.869 \pm 0.015$. Using the Jun et al. (2015) black hole mass estimator based on FWHM(Hα) and L(5100), we derive a black hole mass for WISE J1052+1519 of $\log M_{\rm BH}/M_\odot = 8.61 \pm 0.12$, or $\log M_{\rm BH}/M_\odot = 8.66 \pm 0.13$ using the Jun et al. (2015) estimator based on FWHM(Hα) and L(Hα).

3.2. *SED Modeling*

[*Roberto: Multi-epoch SED modeling, which will presumably indicate fading over obscuration as the primary cause of the dramatic optical spectral changes. Think about related Figure(s).*]

4. PHYSICAL SCENARIOS FOR ABRUPT AGN FADING

In this section, we discuss likely explanations for our observations and we make testable predictions for each of the models we outline. There are two broad categories of explanation for our observations: obscuration and changes to the inner disk.

[2] http://www.asdc.asi.it/mmia/index.php?mission=swiftmastr

4.1. *Obscuration*

First we consider dimming of the central continuum due to obscuration along the sightline. On one hand, if there is no time-lag between the drop in the optical/UV ('high energy') continuum and the reprocessed IR ('low energy') continuum, then the obscurer must lie at some distance from the reprocessing region. The size of the obscurer and the odds of an eclipse-event obscuring half of the low-energy region drop rapidly the further the obscurer is from the low-energy region. On the other hand, if there is a time-lag between the drop in the high-energy and low-energy continua, an obscuration model implies an obscurer lying between the high energy and low-energy regions. Based on our observations, such an obscurer needs to hide $\sim 1/2$ of the high-energy continuum from the reprocessing region and $\sim$ all of the high-energy continuum from our sightline. A large-scale change in the nature of the inner disk could do this (see below), but a typical broad-line region cloud ($N_H \sim 10^{21-22}$cm^{-2}, REF) will not reduce the 2-10keV X-ray continuum by an order of magnitude. We therefore think obscuration independent of inner disk changes is unlikely as a cause of the observed effects.

4.2. *Changes to the Inner disk*

For possible explanations involving the gas disk, we need estimates of the relevant timescales for processes at small radii. Four timescales are important to consider for our purposes. The orbital timescale in the accretion disk is approximately $t_{\rm orb} \sim 1/\Omega$ where $\Omega = \sqrt{GM_{\rm SMBH}/R^3}$ is the Keplerian orbital angular frequency. The thermal timescale in the disk is $t_{\rm th} \sim t_{\rm orb}/\alpha$, where α is the disk viscosity parameter (Shakura & Sunyaev 1973). Cooling and heating front timescales cross the disk on timescales of $t_{\rm front} \sim (h/R)^{-1} t_{\rm th}$, where h/R is the disk aspect ratio, with R the disk radius and $h = c_s/\Omega$ the disk height, with c_s the local disk sound speed at radius R. The viscous disk timescale is written as $t_\nu = (h/r)^{-2} t_{\rm th}$.

Let us assume a SMBH of mass $M_{\rm SMBH} = 3 \times 10^8 M_\odot$ and luminosity $L \sim 0.032 L_{\rm Edd}$ (REF), where $L_{\rm Edd}$ is the Eddington luminosity. Then, the characteristic distance scale is $r_g = GM_{\rm SMBH}/c^2 \sim 4.5 \times 10^{11}$m ($\sim$ 3AU). Assuming $L = \eta \dot{M} c^2$ is the luminosity due to accretion, where $\eta \sim 0.1$ is the luminosity efficiency of accretion, the characteristic mass-flow rate is

$$\dot{M}_{\rm SMBH} \approx 0.2 \frac{M_\odot}{yr} \left(\frac{\eta}{0.1}\right)^{-1} \left(\frac{M_{\rm SMBH}}{3\times10^8 M_\odot}\right) \left(\frac{L_{\rm Edd}}{0.032}\right). \quad (1)$$

Assuming a standard (relatively) thin-disk AGN model consisting of multiple annuli at temperatures that drop with radius, where the mass flow rate across each annulus is $\dot{M}_{\rm SMBH} = 3\pi\nu\Sigma$ and ν is the viscosity, the disk temperature drops as $T \propto r^{-3/4}$ (REFs). The effective disk temperature (the observed 'photosphere' or surface of the disk) is at temperature $T_{\rm eff}^4 \sim T^4/\tau$ where $\tau = \kappa\Sigma$ and κ is the opacity parameter. In order for the observed high-energy flux to drop dramatically at ≤ 3500 requires the thin-disk luminosity at $R < 150 r_g$ to drop by ~ 2 orders of magnitude. If some small UV flux persists, the thin disk luminosity at $R < 150 r_g$ can drop by an order of magnitude.

We can parameterize the relevant disk timescales at $R \sim 150 r_g$ as:

$$t_{\rm orb} \sim 1{\rm month} \left(\frac{R}{150 r_g}\right)^{3/2} \frac{r_g}{c} \quad (2)$$

$$t_{\rm th} \sim 3{\rm yr} \left(\frac{\alpha}{0.03}\right)^{-1} \left(\frac{R}{150 r_g}\right)^{3/2} \frac{r_g}{c} \quad (3)$$

$$t_{\rm front} \sim 60{\rm yr} \left(\frac{h/R}{0.05}\right)^{-1} \left(\frac{\alpha}{0.03}\right)^{-1} \left(\frac{R}{150 r_g}\right)^{3/2} \frac{r_g}{c} \quad (4)$$

$$t_\nu \sim 1200{\rm yr} \left(\frac{h/R}{0.05}\right)^{-2} \left(\frac{\alpha}{0.03}\right)^{-1} \left(\frac{R}{150 r_g}\right)^{3/2} \frac{r_g}{c}. \quad (5)$$

Evidently, since we observe changes on timescales of years in this source, any changes in the disk must be occurring on the thermal or dynamical timescales and are unlikely to be due to viscous effects or propagation of cooling/heating fronts in the inner disk.

4.3. *Causes of changes in inner disk*

Changes in the innermost disk can occur due to occasional instabilities or local perturbations due to objects or events locally or elsewhere in the disk.

4.3.1. *Disk Instabilities*

Disk instabilities can occur for a variety of reasons and on a range of timescales (e.g. Shakura & Sunyaev 1976; Lightman & Shapiro 1976). A classic, short timescale instability is due to an instability in $(\Sigma, T_{\rm eff})$ parameter space due to large changes in opacity from recombination as a result of small changes in Σ (e.g. Lin & Shields 1986). In this case $\dot{\Sigma}$ changes locally so that the local disk lies on the unstable part of the $(\Sigma, T_{\rm eff})$ parameter space S-curve. Once this happens, $T_{\rm eff}$ can drop by an order of magnitude on approximately the thermal timescale $t_{\rm th}$ (or some small multiple thereof, Shakura & Sunyaev (1976). Since the midplane temperature T is approximately unchanged, but $T^4 = \tau T_{\rm eff}^4$, τ can increase dramatically.

4.3.2. *Perturbations due to objects/events*

Changes in the inner disk state can occur due to the presence of local perturbers, such as an extreme mass ratio inspiral (EMRI) event, or more distant changes in the accretion flow. A change in the local value of $\dot{\Sigma}$, which promotes instabilities in $(\Sigma, T_{\rm eff})$ such as those described above, might occur due to embedded supernovae in AGN disks (McKernan et al. 2014, 2017), or stalling of inmigrating objects (J. et al. 2016).

A large population of stellar mass black holes, stellar remnants and stars are expected in AGN disks (e.g. Syer et al. 1991; Artymowicz et al. 1993; McKernan et al. 2012). Torques from gas in the disk causes these secondary objects to migrate in the disk and a fraction of the secondaries will end up on the central supermassive black holes in an extreme mass ratio inspiral (EMRI) event. Once a secondary object ends up in the innermost regions of the accretion disk, its mass can become comparable to, or even dominate, the co-rotating disk mass. From eqn. **??**, a stellar mass black holes of $\sim 10 M_\odot$ could dominate the innermost gas flow on a timescale of decades. Therefore the spectral output of the inner disk can change on the timescales of the EMRI.

The decay timescale of an isolated stellar mass black hole around a supermassive black hole is (Peters 1964)

$$t_{GW} \approx \frac{5}{128} \frac{c^5}{G^3} \frac{a_b^4}{M_b^2 \mu_b} (1 - e_b^2)^{7/2} \quad (6)$$

where $M_b = M_{SMBH} + M_2$ is the binary mass, $\mu_b = M_{SMBH} M_2 / M_b$ is the binary reduced mass and (a_b, e_b) are

the initial binary semi-major axis and eccentricity. Re-parameterizing we find

$$t_{GW} \approx 620\mathrm{yr}\left(\frac{\mathrm{a_b}}{10\mathrm{r_g}}\right)^4\left(\frac{\mathrm{M_{SMBH}}}{10^7\mathrm{M_\odot}}\right)\left(\frac{\mathrm{q}}{10^{-6}}\right)^{-1} \quad (7)$$

where $q = M_2/M_{SMBH}$ is the binary mass ratio.

4.4. *Summary*

[*Daniel: Brief summary/conclusion.*]

REFERENCES

Alexander, D. M., Stern, D., Del Moro, A., et al. 2013, ApJ, 773, 125
Artymowicz, P., Lin, D. N. C., & Wampler, E. J. 1993, ApJ, 409, 592
Becker, R. H., White, R. L., & Helfand, D. J. 1995, ApJ, 450, 559
Blanton, M. R., Lin, H., Lupton, R. H., et al. 2003, AJ, 125, 2276
Boller, T., Freyberg, M. J., Trümper, J., et al. 2016, A&A, 588, 103
Burrows, D. N., Hill, J. E., Nousek, J. A., et al. 2005, SSRv, 120, 165
Drake, A. J., Djorgovski, S. G., Mahabal, A., et al. 2009, ApJ, 696, 870
Fabian, A. C. & Terlevich, R. 1996, MNRAS, 280, L5
Gezari, S., Hung, T., Cenko, S. B., et al. 2017, ApJ, 835, 144
J., J. B., Mac Low, M., McKernan, B., & Ford, K. E. S. 2016, ApJ, 819, L17
Jun, H. D., Im, M., Lee, H. M., et al. 2015, ApJ, 806, 109
Kalberla, P. M. W., Burton, W. B., Hartmann, D., et al. 2005, A&A, 440, 775
LaMassa, S. M., Cales, S., Moran, E. C., et al. 2015, ApJ, 800, 144

Facilities: CRTS, NEOWISE, Palomar (DBSP), SDSS, WISE

Lang, D. 2014, AJ, 147, 108
Lang, D., Hogg, D. W., & Schlegel, D. J. 2016, AJ, 151, 36
Lightman, A. P. & Shapiro, S. L. 1976, ApJ, 203, 701
Lin, D. N. C. & Shields, G. A. 1986, ApJ, 305, 28
Macleod, C. L., Ross, N. P., Lawrence, A., et al. 2016, MNRAS, 457, 389
Mainzer, A., Bauer, J., Grav, T., et al. 2014, ApJ, 784, 110
Martin, D. C., Schiminovick, D., Barlow, T. A., et al. 2005, ApJ, 619, L1
Massey, P. & Gronwall, C. 1990, ApJ, 358, 344
McKernan, B., Ford, K. E. S., Bellovary, J., et al. 2017, MNRAS, submitted (arXiv:1702.07818)
McKernan, B., Ford, K. E. S., Kocsis, B., Lyra, W., & Winter, L. M. 2014, MNRAS, 441, 900
McKernan, B., Ford, K. E. S., Lyra, W., & Perets, H. B. 2012, MNRAS, 425, 460
Peters, P. C. 1964, Phys. Rev., 136, 1224
Risaliti, G., Elvis, M., & Nicastro, F. 2002, ApJ, 571, 234
Roming, P. W. A., Kennedy, T. E., Mason, K. O., et al. 2005, SSRv, 120, 95
Schlafly, E. F. & Finkbeiner, D. 2011, ApJ, 737, 103
Shakura, N. & Sunyaev, R. A. 1973, A&A, 24, 337
—. 1976, MNRAS, 175, 613
Shen, Y., Richards, G. T., Strauss, M. A., et al. 2011, ApJS, 194, 45
Skrutskie, M. F., Cutri, R. M., Stiening, R., et al. 2006, AJ, 131, 1400
Stathakis, R. A. & Sadler, E. M. 1991, MNRAS, 250, 786
Stern, D., Graham, M. J., Arav, N., et al. 2017, ApJ, 839, 2
Syer, D., Clarke, C., & Rees, M. J. 1991, MNRAS, 250, 505
Van Dyk, S. D., Weiler, K. W., Sramek, R. A., & Panagia, N. 1993, ApJ, 419, 69
Wright, E. L., Eisenhardt, P. R. M., Mainzer, A. K., et al. 2010, AJ, 140, 1868